Linear viscoelasticity and thermorheological simplicity of *n*-hexadecane fluids under oscillatory shear *via* non-equilibrium molecular dynamics simulations

Huan-Chang Tseng,*[a] Jiann-Shing Wu[b] and Rong-Yeu Chang[c]

Received 21st September 2009, Accepted 2nd February 2010
First published as an Advance Article on the web 9th March 2010
DOI: 10.1039/b919672b

A small amplitude oscillatory shear flows with the classic characteristic of a phase shift when using non-equilibrium molecular dynamics simulations for *n*-hexadecane fluids. In a suitable range of strain amplitude, the fluid possesses significant *linear viscoelastic* behavior. *Non-linear* viscoelastic behavior of strain thinning, which means the dynamic modulus monotonously decreased with increasing strain amplitudes, was found at extreme strain amplitudes. Under isobaric conditions, different temperatures strongly affected the range of linear viscoelasticity and the slope of strain thinning. The fluid's phase states, containing solid-, liquid-, and gel-like states, can be distinguished through a criterion of the viscoelastic spectrum. As a result, a particular condition for the viscoelastic behavior of *n*-hexadecane molecules approaching that of the Rouse chain was obtained. Besides, more importantly, evidence of *thermorheologically simple* materials was presented in which the relaxation modulus obeys the time–temperature superposition principle. Therefore, using shift factors from the time–temperature superposition principle, the estimated Arrhenius flow activation energy was in good agreement with related experimental values. Furthermore, one relaxation modulus master curve well exhibited both transition and terminal zones. Especially regarding non-equilibrium thermodynamic states, variations in the density, with respect to frequencies, were revealed.

I. Introduction

Linear viscoelasticity is of critical importance in understanding experiments and theories of rheological science. As a rule, such behavior is discussed in the aspect of small amplitude oscillatory shear flows, especially for a wide variety of biomolecular and polymeric materials/fluids.[1–7] It is required to observe a classical feature of oscillatory shear—a phase shift occurring between shear strain and shear stress periodic waves. The fact that the dynamic modulus is not a function of strain amplitude while the Lissajous loop is a elliptic shape[5,8] is called linear viscoelasticity of fluids. Relaxation modulus curves at different temperatures obey the time–temperature superposition principle,[9–11] which is known as *thermorheological simplicity*.[3,12–14]

Recent advances in non-equilibrium molecular dynamics (NEMD) methodology[15–17] have made it possible to engage in academia and industry *via* microscopic understanding of observed macroscopic phenomena for rheological properties. Simple fluids, including argon,[18,19] *n*-alkane,[20–27] and water,[28,29] are generally deemed Newtonian fluids for traditional experimental procedures. Unexpectedly, in NEMD simulations performed on a molecular scale, those fluids also exhibit the so-called non-Newtonian flow, such similarities as shear thinning and normal stress behaviors.[21,27,29,30] Most NEMD studies have been limited to investigating steady state shear[21,27,30,31] and elongation[32–34] flow fields. Apart from a few noteworthy reports, oscillatory shear flow research on both linear viscoelastic and thermorheological simplistic features has *not* yet been presented to any great degree. Hence, the majority of studies have focused on only a few aspects of both features.[35–40]

The dynamic modulus, including storage and loss moduli, G' and G'', is essential in viscoelastic knowledge of various materials in dynamic mechanisms; both moduli with respect to frequency ω, $G'(\omega)$ and $G''(\omega)$, are called the dynamic/viscoelastic spectrum. According to rheological treatises,[2,5,7] primary factors for induced variations of viscoelastic properties are, of course, temperature-dependent, pressure-dependent, and molecular structure-dependent.

It is important to recognize the phase state of fluids on the microscale. Through the dynamic spectrum in a wide range of frequencies,[5,6] several NEMD studies[35–37,41] have determined solid-, liquid-, and gel-like states of fluids under oscillatory shear. A glass transition temperature,[11] T_g, is a key parameter in polymeric physical science. Yoshimoto *et al.*[36] obtained the value of Tg for free-standing polymer thin films from plots of G' and G'' against temperature, performed by NEMD simulations.

From comparisons with theoretical predictions, Cifre *et al.*[35] and Vladkov and Barrat[38] showed that oscillated finite extensible non-linear elastic (FENE) chains closely resembled the Rouse model chains. In addition, Cifre *et al.*[35] and Guo and Jhon[37] adopted NEMD simulations to verify the well-known Cox–Merz rule in the experimental field of polymeric rheology.[2,7]

[a] *Molecular Dynamics Technology Co. Ltd., Hsinchu, 30265, Taiwan. E-mail: ivortseng@moldex3d.com*
[b] *Department of Applied Chemistry, National Chiao Tung University, Hsinchu, 30010, Taiwan*
[c] *Department of Chemical Engineering, National Tsing Hua University, Hsinchu, 30043, Taiwan*

Often quite complex and macromolecular chains need to be specifically modelled using coarse-grained molecular dynamic (CGMD) simulations. Through dissipative particle dynamics (DPD) simulations, Raos *et al.*[42] determined the filled rubber viscoelasticity of polymer network, containing stiff and roughly spherical colloidal particles at a 20% volume fraction. Tao *et al.*[40] developed a multiparticle collision (MPC) dynamics model to investigate the rheological properties of viscoelastic fluids *via* the mesoscopic hydrodynamics method. Borzsák and Cummings[43] adopted the extended simple point charge (SPC/E) model to examine the viscoelastic behavior of water molecules under oscillation. Chen *et al.*[44] employed Brownian dynamics (BD) simulations to monitor "one DNA molecule" undergoing oscillatory pressure-driven flow in microfluid channels.

When reviewing the aforementioned NEMD literature, most have been limited with respect to "constant-volume" NEMD systems.[27] However, the applications of NEMD simulations may not be convenient experimentally because the related experimental data are usually measured under "isobaric conditions". Regrettably, only a few attempts have been made to probe "constant-pressure" NEMD simulations. The reason is the numerical instability: the instantaneous pressure drifts suddenly to generate large instantaneous volume fluctuations. Nevertheless, in order to resolve this issue, Wang and Fichthorn[45] proposed a modified pressure equation to obtain an effectively stable numerical solution of the volume. Thus far, constant-pressure NEMD simulations for oscillatory shear flows have *not* been fairly performed. Therefore, we implement a useful simulation framework that should be applicable to NEMD methodology.

In this study, our fluid of interest, *n*-hexadecane, is one of the more commonly used fluids in surface force apparatus[46,47] (SFA) for lubrication and tribological experiments. The *n*-hexadecane molecule related to the polymer chain is quite short, and should be properly considered as the Newtonian fluid in macroscopic perspective. At a molecular level, most NEMD studies[20,21,27,48] have corroborated that liquid *n*-hexadecane obviously exhibits certain non-Newtonian manifestations.

Recently, we reported[27,49,50] a whole series of NEMD papers in detail, regarding non-thermodynamic and rheological behaviors of *n*-hexadecane fluids under steady-state shear flow, which include shear dilatancy, shear thinning, and normal stress effect. The *original motivation* of the present study is, therefore, geared to "oscillatory shear" extended from steady-state shear based on previous studies.[27,49,50] The *major objective* is to show *linear viscoelasticity* and *thermo-rheological simplicity*. Also, a phase shift of oscillatory sheared fluids is presented while a non-linear viscoelastic behavior of strain thinning,[51] which indicates the modulus decreased upon increasing strain amplitudes, is revealed.

Consequently, this present article presents three significant results below: (i) a criterion for determining phase states of *n*-hexadecane materials at various temperatures can be suggested by considering the viscoelastic spectrum, with $G' > G''$ signifying a solid-like state, $G' < G''$ a liquid-like state, and $G' = G''$ a gel-like state. Moreover, we obtained certain conditions under which the behavior of *n*-hexadecane molecules was close to that of the Rouse chain.[1,3,6] (ii) The relaxation modulus $G(t)$ curves at different temperatures were reduced to one master curve at the reference temperature *via* shift factors of the time–temperature superposition.[1,9–11] The master curve was analyzed as compared to related viscoelastic experimental results. Furthermore, the Arrhenius flow activation energy can be estimated using the data of shift factor plotted against temperature. (iii) With non-equilibrium thermodynamic states of the oscillatory sheared fluid, we further observed how the density varied with respect to the frequency.

The rest of the article is organized as follows. In section II, we briefly describe the oscillatory shear flow fields, the molecular potential models, simulation techniques, and viscoelastic properties. In section III, we offer a least-squares algorithm for determining the optimal values of the storage and loss moduli and present results for the focuses mentioned above. In section IV, we summarize the main conclusions and provide suggestions for future studies.

II. Simulation details

A detailed potential model and the simulation principle used have been reported previously.[27] Here, we give only a brief description for the sake of completeness. The oscillation shear flow system is introduced and viscoelastic properties are expressed, as follows.

A System prototype

The geometry and dimensions of the oscillatory shear flow system are illustrated in Fig. 1, and are also the same as those used for the steady state shear system in the previous studies.[27,49,50] The simulation box is rectangular and three-dimensional, containing 144 *n*-hexadecane molecules. The flow (*x*-axis) and gradient (*y*-axis) directional sizes (L_x and L_y, respectively) of the system are 3.0 and 4.5 nm, respectively. The periodic boundary condition is adopted in the *z* direction with its size (L_z) of 4.5 nm. Notably, in such an oscillatory shear system, the top-plate moves while the low-plate remains stationary. To perform the oscillatory shear flow, a time-dependent shear strain imposed on NEMD systems is given as a sinusoid form,[2]

$$\gamma(t) = \gamma_0 \sin \omega t, \tag{1}$$

where γ_0 is the strain amplitude, ω is the frequency, and t is a time variable; the shear rate is $\dot{\gamma}(t) = \gamma_0\, \omega \cos \omega t$.

B Molecular potential

A coarse-grain model neglects detailed atomic information but maintains the essence of internal molecular structures. The methylene (CH_2) groups are treated as united atoms (UA) with the use of spherical interaction sites in which hydrogen atoms are not explicitly modelled as distinct atoms. Interaction sites connected together can form molecular chains. This coarse-grain model has been adopted widely in relation to molecular dynamics (MD) simulations, such as those of *n*-alkanes[52] and polyethylene (PE) chains.[53] In the present study, we used the set of realistic potential models reported by Chynoweth and Michopoulos[21,54] (CM). This model is superior to the *transferable potential for phase equilibria*

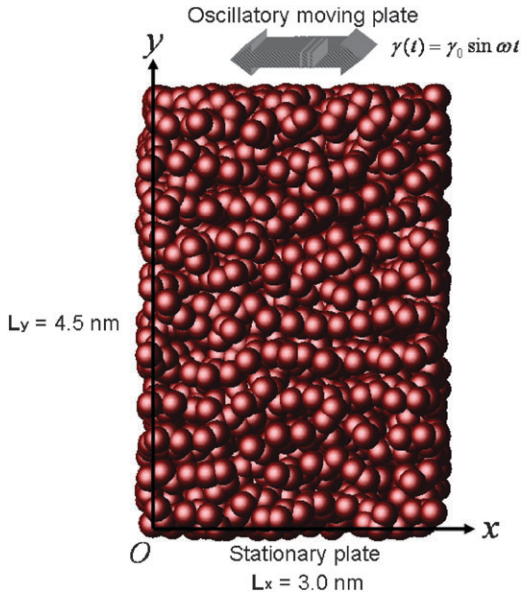

Fig. 1 Schematic representation of the oscillatory shear flow system between a moving upper plate and a stationary lower plate with a time-dependent shear strain of a sinusoid form, $\gamma(t) = \gamma_0 \sin \omega t$: (a) L_x = 3.0 nm in the flow direction (x-axis); (b) L_y = 4.5 nm in the gradient direction (y-axis); (c) L_z = 4.5 nm in the periodic boundary condition direction (z-axis).

(TraPPE) model, which we previously used to examine *n*-hexadecane, when predicting rheological properties.[27] Such a model has been applied in the shear flow[27,55–57] and contraction flow[58] portions of MD simulations. In descriptions of the molecular chains below, the CM model is dominated by van der Waals (vdW) and covalent bonding interactions:

(i) van der Waals interaction. The vdW interaction occurs between CH_2 groups of different chains and also between CH_2 groups in the same chain that are separated by more than *three* CH_2 groups. The vdW interaction can be described by the 12-6 Lennard-Jones (LJ) potential,[21]

$$U_{LJ} = 4\varepsilon_{LJ}\left[\left(\frac{\sigma_{LJ}}{r_{ij}}\right)^{12} - \left(\frac{\sigma_{LJ}}{r_{ij}}\right)^{6}\right], \qquad (2)$$

where r_{ij} is the distance between two CH_2 groups, and ε_{LJ} and σ_{LJ} are the energy and length parameters of the LJ potential, respectively, for the pair of groups i and j. To reduce computational time to determine the vdW force, the shifted LJ potential[15] is usually truncated at a cutoff distance r_c ($r_c = 2.5\,\sigma_{LJ} \approx 10.113$ Å) so that $U_{LJ}(r_c) = 0$.

(ii) Covalent bonding interaction. The bond stretching potential[59] U_s connects two CH_2 groups by harmonic potential with an *equilibrium bond length* l_0 of 1.53 Å,[54]

$$U_s = \tfrac{1}{2}k_l(l_i - l_0)^2, \qquad (3)$$

where k_l is the bond stretching energy constant and l_i is the bond length between two adjacent CH_2 groups.

Table 1 Potential parameters of the Lennard-Jones and covalent bonding interactions

Parameter		Value[a]	Unit
Lennard-Jones	σ_{LJ}	4.045	Å
	ε_{LJ}	0.420	kJ mol^{-1}
Bond stretching	k_l	2650.98	kJ mol^{-1} Å^{-2}
	l_0	1.53	Å
Bond bending	k_θ	0.1004	kJ mol^{-1} deg^{-2}
	k'_θ	0.0096	Deg^{-1}
	θ_0	109.47	Deg
Torsion	c_0	9.278	kJ mol^{-1}
	c_1	12.155	kJ mol^{-1}
	c_2	−13.119	kJ mol^{-1}
	c_3	−3.060	kJ mol^{-1}
	c_4	26.239	kJ mol^{-1}
	c_5	−31.493	kJ mol^{-1}

[a] Lennard-Jones potential parameters (σ and ε) were taken from ref. 21; equilibrium bond length and bond angle (l_0 and θ_0) were taken from ref. 54; bond stretching and bond bending force constants (k_l, k_θ and k'_θ) were taken from ref. 59; torsion potential parameters were taken from ref. 60.

The bond bending potential[59] U_b is described by the Taylor series' cubic term expansion of the bending angle deviation with an *equilibrium bond angle* θ_0 of 109.47°,[54]

$$U_b = \frac{1}{2}k_\theta[(\theta_i - \theta_0)^2 - k'_\theta(\theta_i - \theta_0)^3], \qquad (4)$$

where k_θ is the bond bending energy constant, k'_θ is the bond bending angle constant, and θ_i is a bond angle among three adjacent CH_2 groups.

The torsion potential U_t is expressed by a fifth-order cosine polynomial of a dihedral angle,[60]

$$U_t = c_0 + c_1\cos\phi_i + c_2\cos^2\phi_i + c_3\cos^3\phi_i + c_4\cos^4\phi_i + c_5\cos^5\phi_i, \qquad (5)$$

where $\{c_n\}$ is the value of the set of torsion energy coefficients and ϕ_i is the dihedral angle formed by the four consecutive CH_2 groups. All parameters for the potential models are listed in Table 1.

C Simulation principle

The original NEMD algorithm[15,17,61] was developed by combining SLLOD[17,61,62] equations of motion with the Lees–Edwards sliding brick periodic boundary condition.[63] The algorithm contains two thermodynamic systems: the isochoric–isothermal system (*NVT*-NEMD) and the isobaric–isothermal system (*NPT*-NEMD). Here, we performed the so-called oscillatory shear NEMD simulations under isothermal conditions involving both constant-volume and constant-pressure systems. For overall simulations, we chose the *atomic version*,[27,64,65] including SLLOD equations, temperature, and stress tensor.

The SLLOD equations are ordinary differential equations and are implemented using the numerical method—the Leapfrog–Verlet scheme[66]—which offers a fast-converging iterative algorithm for the Gaussian thermostat multiplier.[20] In addition, the stability and convergence of numerical methods strongly depend on the magnitude of time step, dt. The Courant–Friedrichs–Lewy condition,[67] which is a necessary condition for convergence while solving differential equations

numerically, means that dt is *inversely* proportional to a characteristic velocity U.

In oscillatory shear flows, U is *directly* proportional to the strain amplitude γ_0 and the frequency ω, so that $dt \propto \gamma_0^{-1}$ and $dt \propto \omega^{-1}$ are true. Referring to the NEMD study of Berker *et al.*,[20] the criterion for setting dt is addressed as follows: (i) under a constant frequency of 6.28×10^{11} rad s^{-1}, if $\gamma_0 \leq 0.1$, then $dt = 1.0$ fs, whereas if $\gamma_0 > 0.1$, then $dt \propto \gamma_0^{-1}$; and (ii) under a constant strain amplitude of 0.05, if $\omega \leq 6.28 \times 10^{11}$ rad s^{-1}, then $dt = 1.0$ fs, whereas if $\omega > 6.28 \times 10^{11}$ rad s^{-1}, then $dt \propto \omega^{-1}$. To obtain time averages of the statistical properties, we collected original data every 50 time steps during the run processes. Each NEMD simulation of oscillatory shear was run with 200 cycles of shear strain.

As for the rest of simulation technologies, we used the *ad hoc* velocity rescaling method to stabilize the instantaneous temperature to the desired temperature.[15] In the constant pressure NEMD system, to provide an effectively stable numerical solution of the volume, we adopted a simple modified pressure equation of Wang and Fichthorn's.[45] Detailed information regarding the aforementioned equations and algorithms are available elsewhere.[27]

D Viscoelastic property

For an atomic system, an xy component of the stress tensor τ_{yx} is given by the Irving–Kirkwood equation,[15,68]

$$\tau_{yx} = -\frac{1}{V}\left(\sum_{i=1}^{N}\frac{p_{ix}p_{iy}}{m_i} + \sum_{i=1}^{N}\sum_{j>i}^{N} r_{ijx}f_{ijy}\right), \quad (6)$$

where $\mathbf{p}_i$ is the momentum of the ith atom; p_{ix} and p_{iy} are components of $\mathbf{p}_i$; m_i is the mass of the ith atom; r_{ij} denotes the distance vector from atom j to atom i; f_{ij} denotes the force imposed on atom i due to atom j; N equals the total number of atoms; V is the system volume; and the superscript xy denotes the x- and y-axes as the flow and gradient directions of the flow system, respectively.

In an oscillatory shear flow, the phase shift exists between the τ_{yx} and γ waves:

$$\tau_{yx} = \tau_0 \sin(\omega t + \delta), \quad (7)$$

where τ_0 is the stress amplitude and δ is the phase angle.

The material functions, *i.e.*, the elastic or storage shear modulus G' and the viscous or loss shear modulus G'', are usually represented as follows:

$$\tau_{yx}/\gamma_0 = G_d \sin(\omega t + \delta) = G'(\omega)\sin\omega t + G''(\omega)\cos\omega t, \quad (8)$$

$$\tan\delta = G''/G', \quad (9)$$

where G_d is the amplitude ratio (τ_0/γ_0) and $\tan\delta$ is the loss tangent.

G' and G'', which depend on G_d and δ, are also known as *dynamic modulus*: $G' = G_d \cos\delta$ is related to the elastic energy stored in fluids and $G'' = G_d \sin\delta$ is related to the energy dissipated by the viscous flow. Regarding rheological states of fluids, notice that $\delta = 0$ and $\delta = \pi/2$ signify the behavior of a Hookean solid (linear, purely elastic) and Newtonian fluid (linear, purely viscous), respectively; thus, $0 < \delta < \pi/2$ indicates viscoelastic materials.[5] To obtain G' and G'', in the next section, we simply describe how to determine the optimal value of G_d and δ by using the least-squares algorithm.[69]

III. Results and discussion

To prove both *linear viscoelasticity* and *thermorheologically simple* characteristics of the fluid, *n*-hexadecane under oscillatory shear, we have organized significant discussions into four sections, as follows. In section IIIA, the phase shift is substantially presented and the method for determining both optimal storage and loss moduli is proposed with concreteness. In section IIIB, we validate that the fluid possessed a linear viscoelastic behavior through two representations of viscoelastic properties. In section IIIC, the temperature-induced variation in both viscoelastic behaviors and phase states of the fluid makes for detailed discussions. In section IIID, we establish the thermorheological simplicity of the fluid in that its relaxation modulus curves at different temperatures obeys the time–temperature superposition principle[1,9–11] and then yield a master curve at a reference temperature. In addition, the Arrhenius flow activation energy can be estimated by shift factors of the principle.

A Oscillatory shear

Referring to related treatises of polymeric viscoelasticity,[1,2,5] oscillatory shear flow is observed when a time-dependent shear strain $\gamma(t)$ imposes on fluids with sinusoidal function. As a result, the response of the fluid's shear stress $\tau_{yx}(t)$ is also considered a sinusoidal wave with respect to time. Very importantly, it is necessary to find the optimal value of G_d and δ to determine storage and loss moduli.

1. Phase shift. A phase shift, which means the difference between the shear stress and shear strain waves with respect to time, is a fundamental manifestation of oscillatory shear flow. As a beginning, the data from the shear stress were used in the performance of oscillatory shear NVT-NEMD simulations for *n*-hexadecane fluids at a state point of 477.6 K and 0.896 g cm^{-3}. To confirm the initial exact findings quickly, we chose a higher frequency ($\omega = 6.28 \times 10^{12}$ rad s^{-1}) and a smaller strain amplitude ($\gamma_0 = 0.05$). This run, with $dt = 0.1$ fs, was performed during 200 periods of shear strain, *i.e.*, 200 ps.

Fig. 2 presents the averaged data of shear strain and shear stress waves with respect to a period of sinusoidal function, θ_p $(0 \leq \theta_p \leq 2\pi)$. It is clear that the so-called phase shift is observed with a phase angle of *ca.* 54.9° (or 0.958 rad), as corroborated above. Therefore, this NEMD simulation system is deemed to be a fairly oscillatory shear flow.

2. Dynamic modulus. For the data regarding the shear stress with respect to time, $\tau_{yx}(t)$, using the least-squares method[69] we determined the optimal values of G' and G''. This computational process comprised the following *five steps*:

(i) The phase angle δ between 0 and $\pi/2$ was divided into 100 intervals; the fraction δ_m was given by

$$\delta_m = \frac{\pi}{2 \times 100} m, \quad m = 0, 1, 2 \ldots, 100. \quad (10)$$

(ii) Referring to eqn (7), we defined a *new* variable X_s at δ_m:

$$X_s = \sin(\omega t_s + \delta_m), \; s = 1, 2, 3, \ldots, N_s, \quad (11)$$

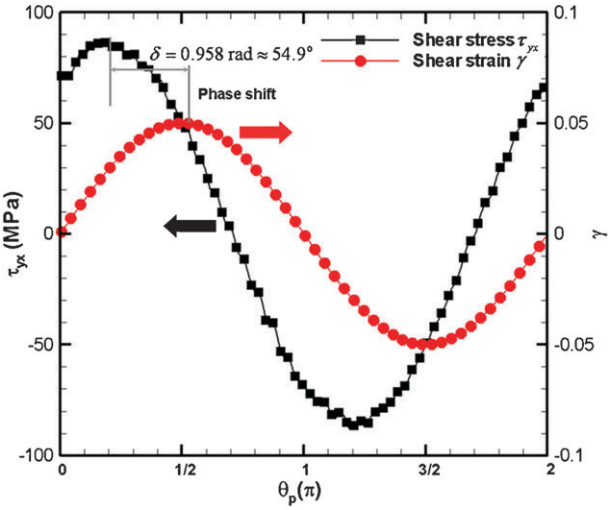

Fig. 2 Phase shift diagram of the shear stress τ_{yx} (left axis) and shear strain γ (right axis) plotted against period of time θ_p for *n*-hexadecane under constant conditions (T = 477.6 K; ρ = 0.896 g cm^{-3}; γ_0 = 0.05; ω = 6.28 × 10^{12} rad s^{-1}). Note that phase angle δ = 0.958 rad ≈ 54.9°.

then,

$$\tau_{yx,s} = \tau_0 X_s, \tag{12}$$

where $\tau_{yx,s}$ is the shear stress of the ith statistical sample and N_s is the total number of statistical samples. Thus, eqn (12) is a *linear* equation. From the known set $\{t_s,\tau_{yx,s}\}_{s=1}^{s=Ns}$, we obtained the set $\{X_s,\tau_{yx,s}\}_{s=1}^{s=Ns}$; additionally, using the least-squares method, the set $\{X_s,\tau_{yx,s}\}_{s=1}^{s=Ns}$ at $\delta = \delta_m$ can be used to find a appropriate value of $\tau_0(\delta_m)$. Due to $G_d = \tau_0/\gamma_0$, the value of $G_d(\delta_m)$ was also determined. Thus, we obtained the set $\{\delta_m,G_d(\delta_m)\}_{m=1}^{m=100}$.

(iii) Using the method from the previous step employed to obtain the set $\{X_s\}_{s=1}^{s=Ns}$, at $\delta = \delta_m$, a particular shear stress $\tau_{yx,s}^{LS}$ was evaluated by the least-squares method,

$$\tau_{yx,s}^{LS}(\delta_m) = \tau_0(\delta_m)X_s. \tag{13}$$

(iv) At $\delta = \delta_m$, a standard deviation $\bar{\varepsilon}$ was defined:

$$\bar{\varepsilon}(\delta_m) = \sqrt{\frac{\sum_{s=1}^{N_s}(\tau_{yx,s}^{LS}(\delta_m) - \tau_{yx,s})^2}{N_s}}. \tag{14}$$

Consequently, we obtained the set $\{\delta_m,\bar{\varepsilon}(\delta_m)\}_{m=1}^{m=100}$.

(v) In steps (ii) and (iv) above, we obtained the sets $\{\delta_m,G_d(\delta_m)\}_{m=1}^{m=100}$ and $\{\delta_m,\bar{\varepsilon}(\delta_m)\}_{m=1}^{m=100}$, respectively. $G_d(\delta_m)$ was plotted against δ_m and $\bar{\varepsilon}(\delta_m)$ against δ_m, as indicated in Fig. 3. Thus, a *minimum* value of $\bar{\varepsilon}$ was found at $\bar{\varepsilon}_{min}$ = 53.26 MPa; also, $\delta_m(\bar{\varepsilon}_{min})$ = 0.958 rad and $G_d(\bar{\varepsilon}_{min})$ = 1704.18 MPa.

Eventually, $\delta_m(\bar{\varepsilon}_{min})$ and $G_d(\bar{\varepsilon}_{min})$ were substituted into $G' = G_d \cos\delta$ and $G'' = G_d \sin\delta$ to obtain values 980.16 and 1394.10 MPa respectively. Thus, tan $\delta = G''/G'$ equalled 1.422 and then the calculated value of δ = 54.89° was also in well agreement with the observed value in Fig. 2. Therefore, we performed this simple program above to determine the optimal values of G' and G'' for the next section.

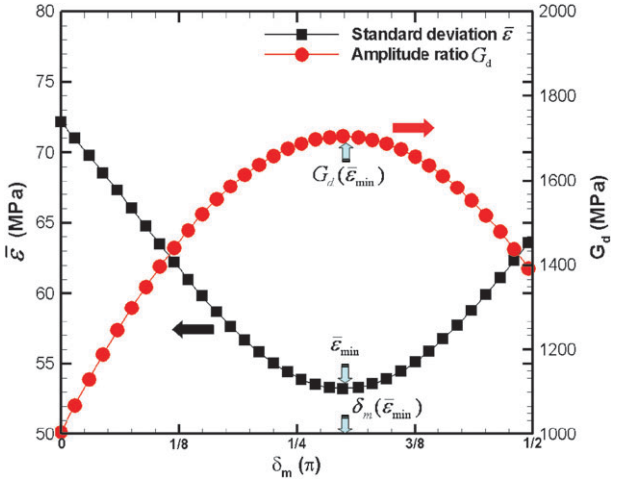

Fig. 3 Standard deviation $\bar{\varepsilon}$ (left axis) and amplitude ratio G_d (right axis) plotted against phase angle δ, obtained using the least-squares method for *n*-hexadecane under constant conditions (T = 477.6 K; ρ = 0.896 g cm^{-3}; γ_0 = 0.05; ω = 6.28×10^{12} rad s^{-1}). Note that $\bar{\varepsilon}_{min}$ = 53.26 MPa, $\delta_m(\bar{\varepsilon}_{min})$ = 0.958 rad, and $G_d(\bar{\varepsilon}_{min})$ = 1704.18 MPa.

B Linear viscoelasticity

As a rule, the linear viscoelastic behavior of fluids occurs in the so-called small strain amplitude oscillatory shear (SAOS) flows. There is, however, a troublesome problem—how small a range of strain amplitude can be considered an SAOS flow field? This issue is resolved below. The first—and major—goal for the present study was to prove that the fluid was a linear viscoelastic fluid. Two significant findings can demonstrate linear viscoelastic characteristics: (i) the Lissajous loop in a suitable range of strain amplitude presents an elliptic loop; and (ii) the storage and loss moduli do not depend on the strain amplitude.

1. Shear stress against shear rate. Plots of shear stress against shear rate ($\tau_{yx} - \dot{\gamma}$) show a variety of elliptic shape, which is known as the Lissajous loop.[5,8,70–72] The loop for the pure elastic fluid is a perfect elliptic loop, whereas that for a pure viscous fluid is reduced to a straight line.[8,10] Thus, the loop for a viscoelastic fluid should be a somewhat narrow elliptical loop, with its long and short axes not aligned parallel to the shear stress and shear rate ones. Notably, Jeyaseelan and Giacomin, who completely reviewed the viscoelastic experiments and theories, suggested that the Lissajous loop is a distorted elliptical for non-linear viscoelastic materials.[72]

Here, the oscillatory *NVT*-NEMD simulations, with γ_0 = 0.05 and ω = 6.28 × 10^{11} rad s^{-1}, were held constant at 477.6 K and 0.896 g cm^{-3} for *n*-hexadecane molecules. In the viscoelastic experiment, Hyun *et al.*,[70] discussed the effect of the strain amplitude on a $\tau_{yx} - \dot{\gamma}$ loop. As shown in Fig. 4, variations in the $\tau_{yx} - \dot{\gamma}$ loop were observed over a wide range of strain amplitudes, $0.001 \le \gamma_0 \le 0.6$; wherein the square and circle symbols are obtained by using NEMD simulation and least-squares method, respectively. The auxiliary for the circle was performed to check whether the simulated loop could be confirmed as a standard elliptical loop.

In Fig. 4(a), the points in the $\tau_{yx} - \dot{\gamma}$ plot at γ_0 = 0.6 obviously indicate a somewhat distorted elliptical loop.

As shown in Fig. 4(a)–(c), the degree of distortion of the elliptical loop decreases as the value of γ_0 is decreased from 0.6 to 0.2, until $\gamma_0 = 0.1$ [Fig. 4(d)], where the $\tau_{yx} - \dot{\gamma}$ plot is almost a standard ellipse. Over a range of strain amplitude, $0.01 \leq \gamma_0 \leq 0.1$, the $\tau_{yx} - \dot{\gamma}$ plots in Fig. 4(d)–(f) remain constant as elliptical loops. When $\gamma_0 = 0.005$ is a very low value, Fig. 4(g) displays that the points in the $\tau_{yx} - \dot{\gamma}$ plot do not form a loop—rather, they disperse slightly. Even when $\gamma_0 = 0.001$ [Fig. 4(h)], the points do not clearly form a loop; this behavior was caused by the strong thermal fluctuation of molecules at such low values of strain amplitude.

Therefore, we tentatively conclude that the fluid possesses linear viscoelastic characteristics in a suitable range of strain amplitudes $0.01 \leq \gamma_0 \leq 0.1$, but non-linear viscoelastic characteristics for $\gamma_0 > 0.1$. In particular, for $\gamma_0 < 0.01$, the points in the $\tau_{yx} - \dot{\gamma}$ plot did exhibit random distributions, and did not remain constant as an elliptical loop.

2. Dynamic modulus against strain amplitude. Related rheological research[1,2,5,6] describes that linear viscoelasticity shows an imposed strain amplitude independence of the storage and loss moduli. Fig. 5 presents plots of G' and G'' against γ_0 over a wide range of strain amplitudes ($0.001 \leq \gamma_0 \leq 0.6$). By using two auxiliary parallel dash lines, it is clear that the values of G' and G'' remain almost constant in the range $0.01 \leq \gamma_0 \leq 0.1$, *i.e.*, G' and G'' are not related to γ_0. In other words, we prove that the linear viscoelastic feature of the fluid occurred in a limited suitable γ_0 range: from 0.1 to 0.01.

In general, non-linear viscoelastic behavior is classified into three types: strain thinning, strain hardening and weak strain overshoot.[51] Returning to Fig. 5, for high strain amplitudes (about $\gamma_0 > 0.1$), the value of G' decreased dramatically upon increasing γ_0; the corresponding decrease in G'' was slight. Such a result reveals an example of strain thinning. In contrast, for low strain amplitudes (about $\gamma_0 < 0.01$), the values of G' and G'' both decreased with the decreasing γ_0; this is due to strong thermal fluctuation of the molecules.

In rheological experiments,[4] one suggested that polymeric fluids at $\gamma_0 < 0.5$ can exhibit linear viscoelastic behavior. In the present study, the range of linear viscoelasticity for *n*-hexadecane fluids, $0.01 \leq \gamma_0 \leq 0.1$, is very reasonable. Therefore, in the next section, we examine the effect of temperature on both the range of strain amplitude for linear viscoelasticity and the slope of strain thinning for non-linear viscoelasticity.

Incidentally, *linear viscoelastic* behavior exploits the *linear response theory*,[17,73] which means that the relaxation of a system following infinitesimal external perturbations is identical to the relaxation from spontaneous fluctuations at equilibrium. Hence, this is why γ_0 must be less than 0.1, to ensure that the chain conformations are always very near equilibrium. Because thermodynamic fluctuation (or a lower signal-to-noise ratio) at a low value of γ_0 (<0.001) results strongly in large statistical uncertainty,[22] the fluid does *not* possess the linear viscoelastic behavior.

C Temperature dependence

In the previous section, we identified the oscillatory shear flow to be a constant-volume NEMD system, although the experiments were generally performed under isobaric conditions. In a previous study,[27] we proved the agreement between *NPT*-NEMD and *NVT*-NEMD simulations for "steady state shear flows." Hence, at present, we also investigated whether such an agreement could also be established for "oscillatory shear flows."

Under the constant oscillatory shear conditions ($T = 400$ K; $\omega = 6.28 \times 10^{11}$ rad s^{-1}; $\gamma_0 = 0.05$), we presented evidence for agreement between the *NPT*-NEMD and *NVT*-NEMD simulations under an oscillatory shear. The geometry and dimension of both simulation systems were the same as those used in Fig. 1. In the *NPT*-NEMD simulations, we used a wide pressure range (1.5–1000 MPa) to obtain converged densities; in the *NVT*-NEMD simulation, we used a wide density range (0.70–0.95 g cm^{-3}) to obtain converged pressures.

As the density–pressure (ρ–P) curves clearly illustrate in Fig. 6, the density increased upon increasing the pressure; this trend is consistent with general physics. Significantly, both the *NPT*-NEMD and *NVT*-NEMD curves were almost superimposed. Coincidentally, the ρ–P data can be formulated using the equation, $\rho = 0.681 + 0.00876\sqrt{P}$, where the unit of ρ and P is g cm^{-3} and MPa, respectively.

These results for oscillatory shear flows underline the equivalence between the *NPT*-NEMD and *NVT*-NEMD simulations under like conditions. In the following section, we treat the oscillatory shear problems in constant pressure systems—namely, the effect of temperature on viscoelastic behaviors.

1. Viscoelastic behavior. We performed oscillatory shear *NPT*-NEMD simulations under constant conditions (250 MPa; $\omega = 6.28 \times 10^{11}$ rad s^{-1}) over a wide range of strain amplitudes (0.0025–0.5) for *n*-hexadecane molecules. Fig. 7 presents plots of G' and G'' against γ_0 at temperatures of 300, 400, and 500 K. As per Fig. 5, two auxiliary parallel lines in Fig. 7 also determine the γ_0 range of linear viscoelasticity: roughly, $0.0075 \leq \gamma_0 \leq 0.75$ at 300 K, $0.01 \leq \gamma_0 \leq 0.1$ at 400 K, and $0.025 \leq \gamma_0 \leq 0.2$ at 500 K. At the same time, the difference between the largest and smallest values of the range can be obtained: 0.675 at 300 K, 0.09 at 400 K, and 0.175 at 500 K. Accordingly, the LVE range lengthened as the temperature rose. In addition, we observed that the gap between the G' and G'' curves also increased with temperature. As a result, the range at high temperatures is long while the gap is wide. Regarding the non-linear viscoelastic behavior, the slope of the strain thinning decreased as the temperature increased. In particular, for the highest temperature of 500 K [Fig. 7(c)], the strain thinning effect was not obvious.

As analyzed above, we chose enough of the small strain amplitude ($\gamma_0 = 0.05$) so that the fluid at different temperatures remained in a constant linear viscoelastic state. Cautiously, we again proved that the $\tau - \dot{\gamma}$ plots at 300, 400, and 500 K were elliptical loops under constant conditions ($P = 250$ MPa; $\gamma_0 = 0.05$; $\omega = 6.28 \times 10^{11}$ rad s^{-1}). Fig. 8 presents the fact that the elliptical loop gradually narrowed as the temperature increased. Up to the highest temperature (500 K), the elliptical loop remained very thin and approximated a line, as shown in Fig. 8(c). Such loops are also in agreement with descriptions of related linear viscoelastic investigations.[5,8,70–72]

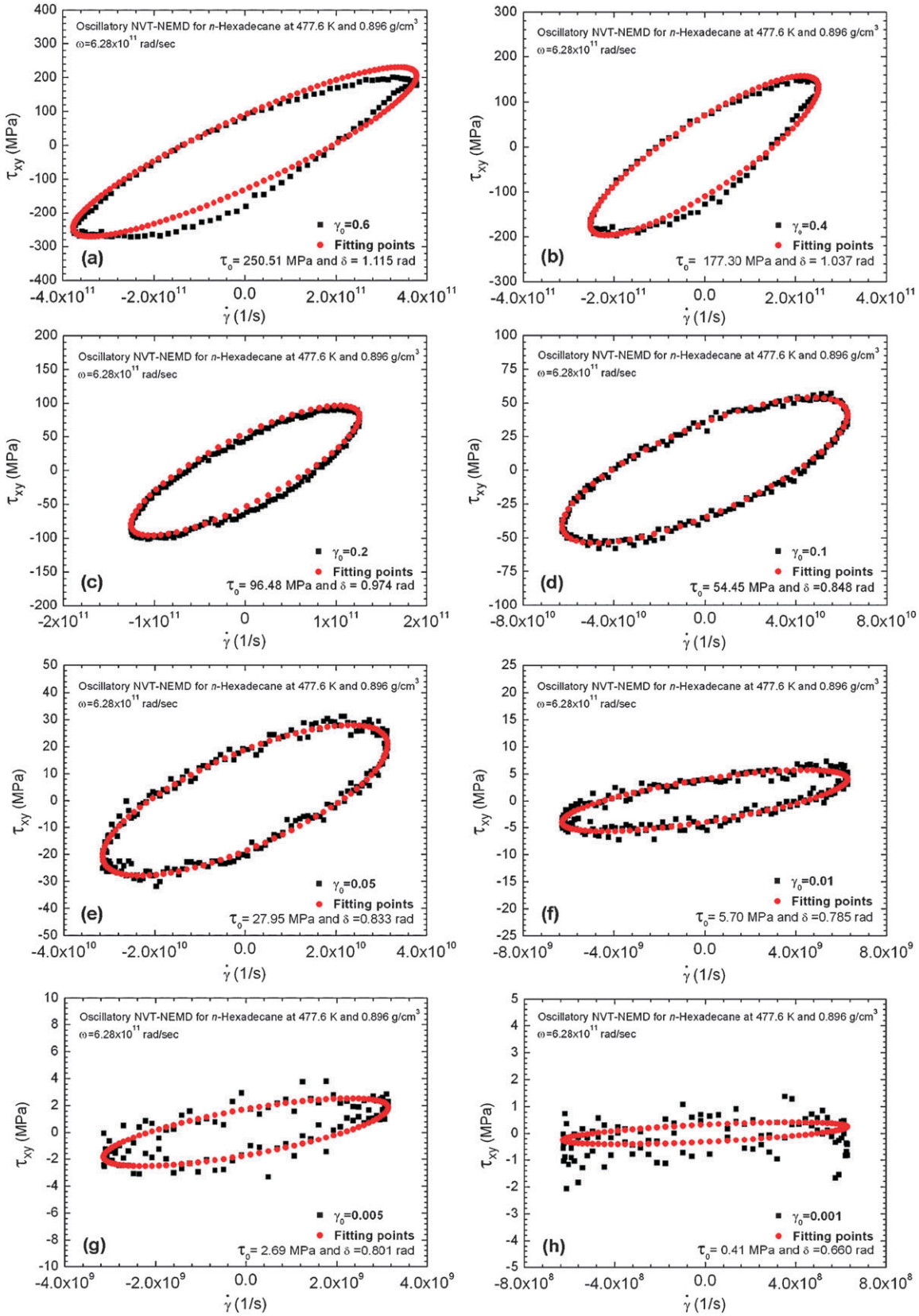

Fig. 4 Lissajous plots of the shear stress τ_{yx} plotted against the shear rate $\dot{\gamma}$ at various strain amplitudes of (a) 0.6, (b) 0.4, (c) 0.2, (d) 0.1, (e) 0.05, (f) 0.01, (g) 0.005, and (h) 0.001, for *n*-hexadecane under constant conditions (T = 477.6 K; ρ = 0.896 g cm^{-3}; ω = 6.28×10^{11} rad s^{-1}). Fitting points are obtained by using the least-squares method.

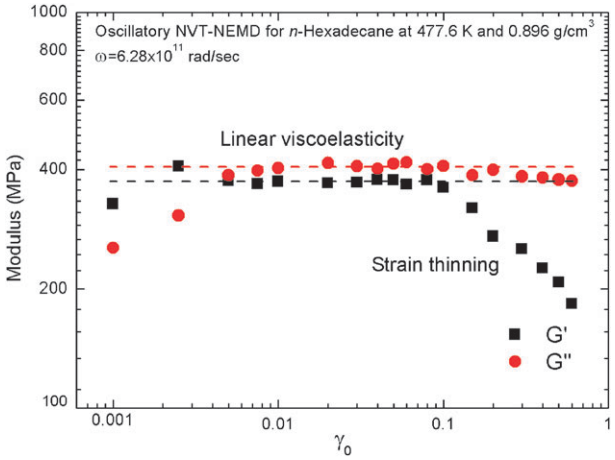

Fig. 5 Storage and loss moduli, G' and G'', plotted against strain amplitude γ_0 for *n*-hexadecane under constant conditions (T = 477.6 K; ρ = 0.896 g cm^{-3}; ω = 6.28 × 10^{11} rad s^{-1}). The dashed line is the auxiliary for estimating the range of linear *viscoelasticity*.

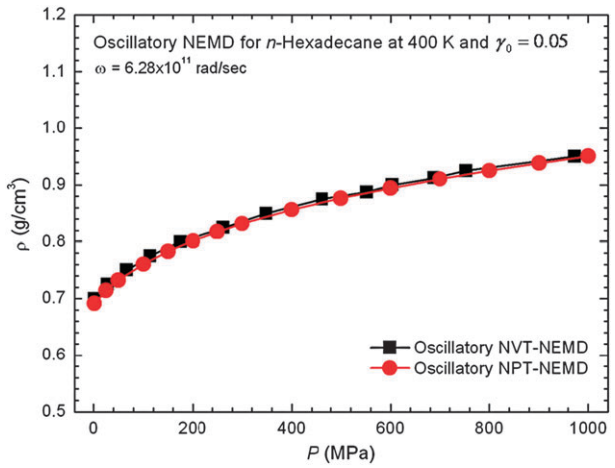

Fig. 6 Plots of the pressure P plotted against the density ρ, obtained from both oscillatory shear *NVT*-NEMD and oscillatory shear *NPT*-NEMD simulations for *n*-hexadecane under constant conditions (T = 400 K; γ_0 = 0.05; ω = 6.28×10^{11} rad s^{-1}).

Moreover, the rheological states are described by phase angles δ of zero for a pure elastic fluid, $\pi/2$ for a pure viscous fluid, and a range between zero and $\pi/2$ for a viscoelastic fluid. Fig. 9 presents the variation in δ with respect to temperature. An intersection appeared near 375 K. Beyond the intersection, δ may approach $\pi/2$, which means that the fluid at high temperatures (>375 K) is close to a pure viscous state; whereas before the intersection, the fluid exists in a viscoelastic state. The vicinity of this intersection point indicates that the transition phase of the fluid varied between viscoelastic to near-viscous behaviors.

2. Viscoelastic spectrum. The effect of temperature strongly influences phase states of materials/fluids. Traditional dynamic experiments[5,6] usually adopt viscoelastic spectra, $G'(\omega)$ and $G''(\omega)$, to distinguish phase states of materials: $G' > G''$ signifies a solid-like state; $G' < G''$, a liquid-like state; and $G' = G''$, a gel-like state. Especially for the gel state, Tung and Dyne[3,5,74] proposed that the crossover of the G' and G'' curves occurred at the gel temperature (also called the gel point). In the present study, we examined the *n*-hexadecane fluid over a wide temperature range, from 250 to 500 K. The range indicated the fluid's phase state varied from solid to liquid due to the melting point[75] and boiling point[21] of *n*-hexadecane being 289–291 and 558 K, respectively.

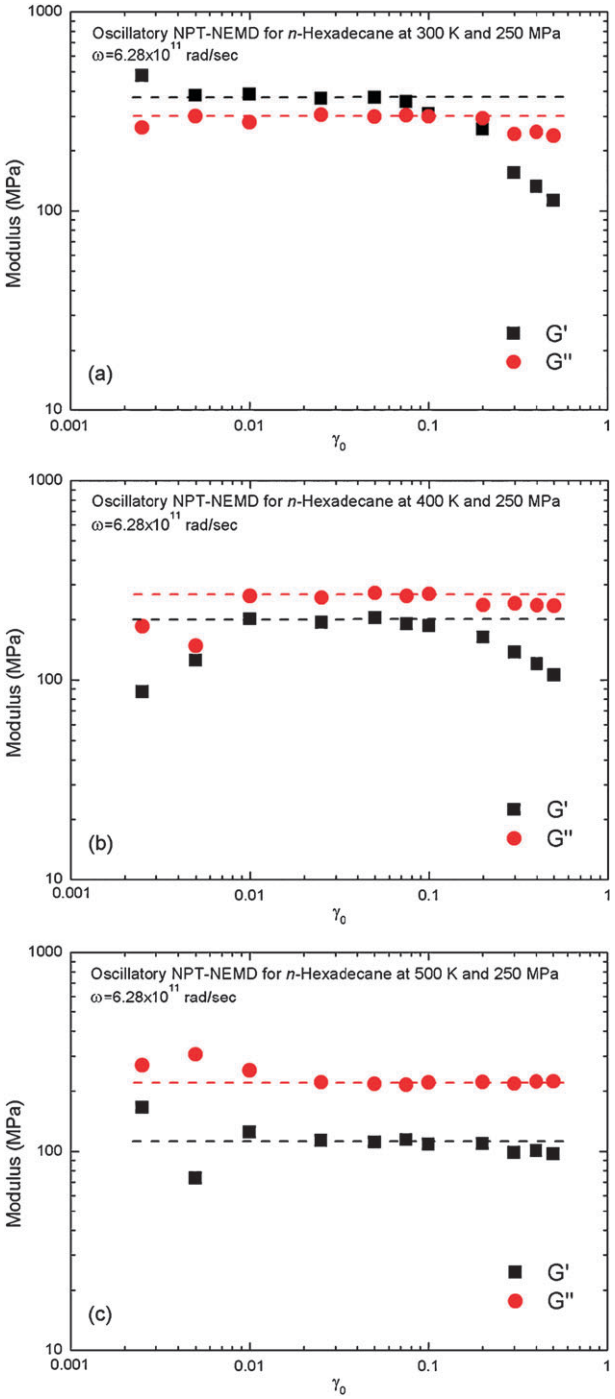

Fig. 7 Storage and loss moduli, G' and G'', plotted against strain amplitude γ_0 at various temperatures of (a) 300, (b) 400, and (c) 300 K, for *n*-hexadecane under constant conditions (P = 250 MPa; ω = 6.28 × 10^{11} rad s^{-1}). The dashed line is the auxiliary for estimating the range of linear *viscoelasticity*.

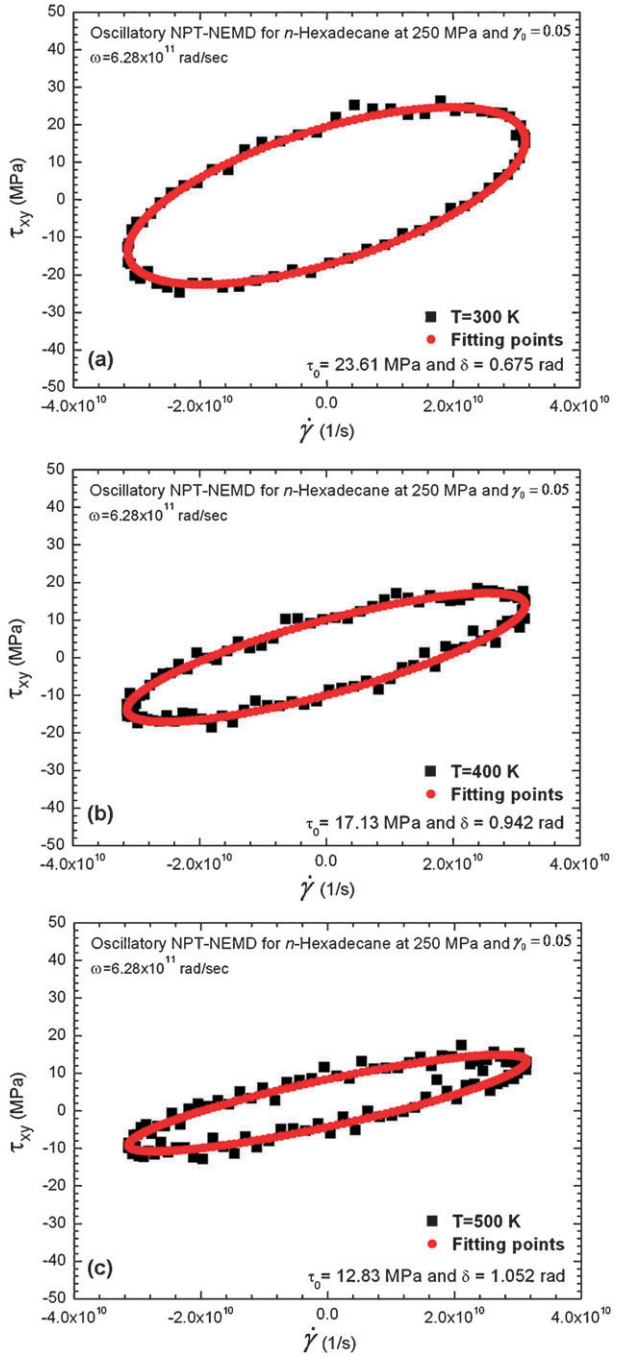

Fig. 8 Lissajous plots of the shear stress τ_{yx} plotted against the shear rate $\dot{\gamma}$ at various temperatures of (a) 300, (b) 400, and (c) 300 K, for *n*-hexadecane under constant conditions (P = 250 MPa; γ_0 = 0.05; $\omega = 6.28 \times 10^{11}$ rad s^{-1}). Fitting points are obtained by using the least-squares method.

Fig. 10 shows plots of $G'(\omega)$ and $G''(\omega)$ at various temperatures (250, 300, 350, 400, 450, and 500 K) over a wide frequency range ($6.28 \times 10^{10} \leq \omega \leq 6.28 \times 10^{12}$ rad s^{-1}). At the lowest temperature (250 K), we conjectured that the material should exist in a solid state. Thus, Fig. 10(a) clearly shows $G' > G''$, which means that the fluid was in a solid-like state. Only at the highest frequency (6.28×10^{12} rad s^{-1}) did $G' \approx G''$, indicating that the fluid was in a gel-like state.

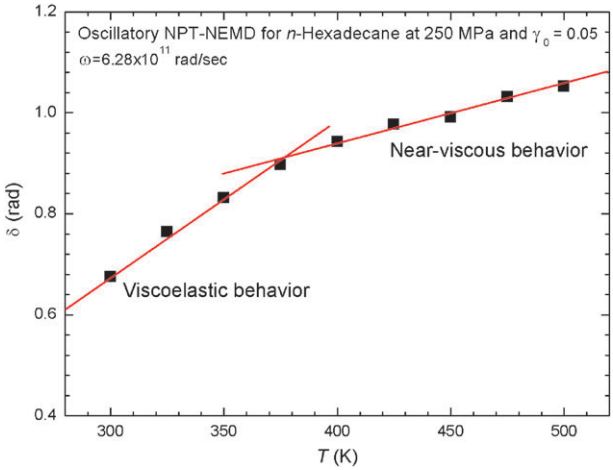

Fig. 9 Phase angle δ plotted against temperature T for *n*-hexadecane under constant conditions (P = 250 MPa; γ_0 = 0.05; $\omega = 6.28 \times 10^{11}$ rad s^{-1}). Note that the two lines are linear fits of the data with an intersection shown near 375 K.

Fig. 10(b) shows that both the G' and G'' curves were almost superimposable at 300 K; namely, the fluid exhibited a gel-like state.

When the temperature rose to 350 K [Fig. 10(c)], a transition point was found near $\omega = 6.28 \times 10^{11}$ rad s^{-1}; before the transition point, $G' < G''$ referencing a liquid-like state; in contrast, the fluid was in a gel-like state after the transition point. Processed to 400 K [Fig. 10(d)], $G' > G''$ over the whole frequency range, signifying that the fluid was in a liquid-like state. As expected, $G' > G''$ at the highest temperatures (450 and 500 K), undoubtedly indicating the liquid-like state of the fluid [Fig. 10(d) and (e)]. In passing, our previous study[50] proved that, by inspecting the overall shape of the intermolecular radial distribution function[15,76,77] (RDF) curves at various temperatures (300–500 K), the *n*-hexadecane fluid can be readily corroborated to exist in the *liquid* state.

More significantly, the variations in the values of G' and G'', with respect to frequency at 350 K in Fig. 10(c), are rather similar to those of the Rouse model chains: at high frequencies, $G' = G'' \propto \omega^{0.5}$; at low frequencies, $G' \propto \omega^{2.0}$ and $G'' \propto \omega^{1.0}$. When we fit the data in Fig. 10(c), we obtain the following two specific situations: (i) beyond the transition points, $G' \propto \omega^{0.52}$ and $G'' \propto \omega^{0.47}$, which is close to the predictions of the Rouse model; and (ii) before the transition points, $G' \propto \omega^{0.73}$ and $G'' \propto \omega^{0.5}$—results that clearly diverge from the Rouse model because of the realistic molecular potential used.

However, by using the FENE model, Cifre *et al.*[35] obtained data that proved NEMD results were in good agreement with the theoretical predictions of the Rouse model. Related experimental observations of the gel point,[5,6] with $G' < G''$, have suggested that $G' \propto \omega^{\alpha}$ for $\alpha > 0.5$. Therefore, our prediction ($G' \propto \omega^{0.73}$) appears to be quite acceptable. Consequently, we could suggest that, at a particular temperature of about 350 K, the *n*-hexadecane fluid possesses viscoelastic behavior while its molecular chain at high frequencies is close to the Rouse chain.

Furthermore, Fig. 10 was arranged to produce both Fig. 11 and 12. As a whole, we observed that the values of

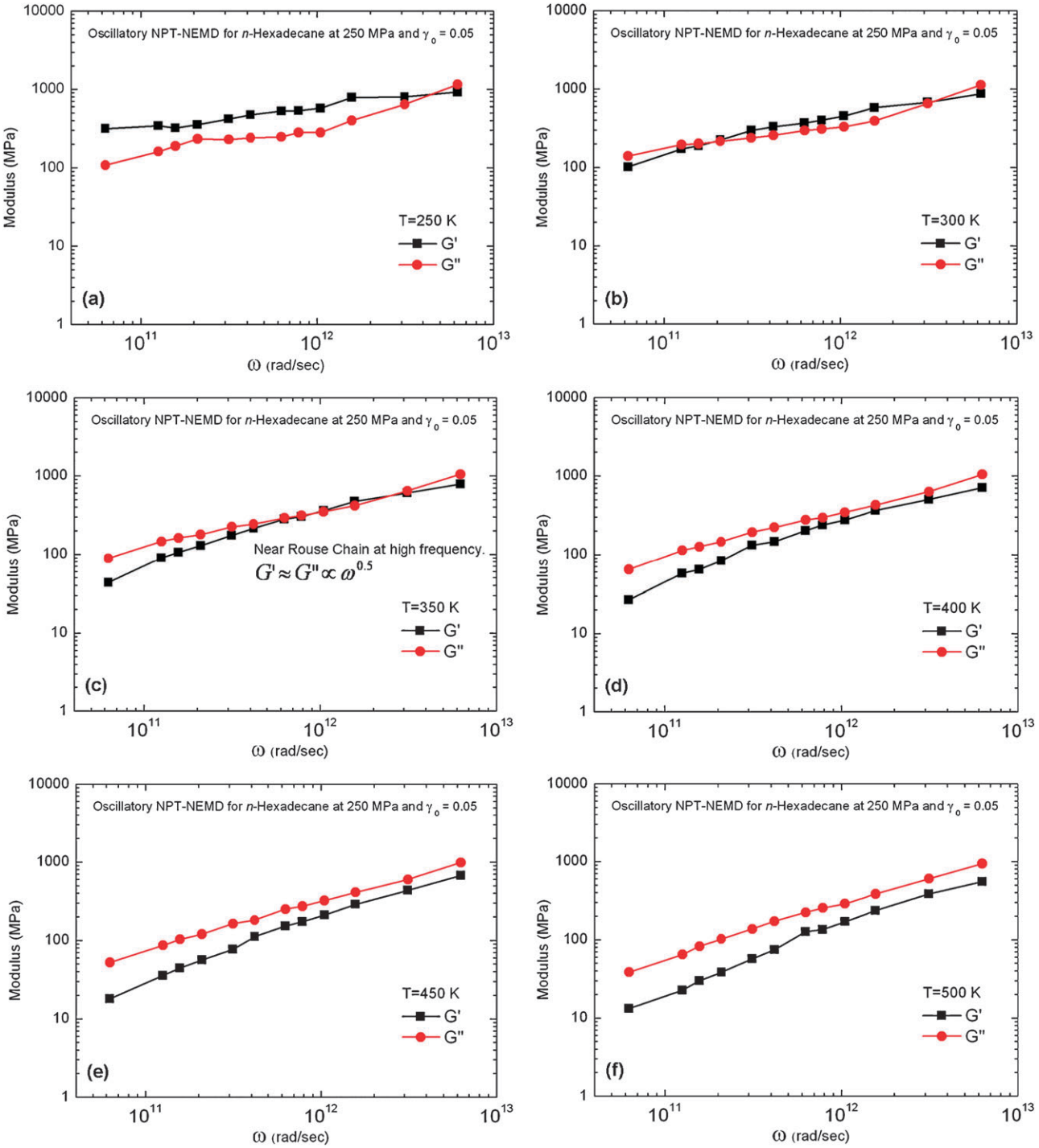

Fig. 10 Storage and loss moduli, G' and G'', plotted against frequency ω at various temperatures of (a) 250, (b) 300, (c) 350, (d) 400, (e) 450, and (f) 500 K, for *n*-hexadecane under constant conditions (P = 250 MPa; γ_0 = 0.05).

G' and G'' both increased with increasing ω, but decreased upon increasing the temperature. Such a result was in qualitative agreement with the findings from related experiments by Yang *et al.*,[78] who adopted atomic force microscopy (AMF) and differential scanning calorimetry (DSC) to investigate the linear viscoelasticity measurements and detected the microphase separation transition for polyurethane (PU) elastomer.

Surprisingly, at higher frequencies ($\omega > 6.28 \times 10^{11}$ rad s^{-1}), all of the $G''(\omega)$ curves closely matched each other, demonstrating the temperature independence of G''. We observed similar characteristics in previous studies.[27,49,50] For example, we found that at high shear rates ($\dot{\gamma} > 1 \times 10^{11.5}$ s^{-1}) the material functions, including η, ψ_1, $-\psi_2$, and $-\psi_2/\psi_1$, did not depend on temperature; wherein η is the viscosity, and ψ_1 and ψ_2 are the first and second normal stress coefficients,

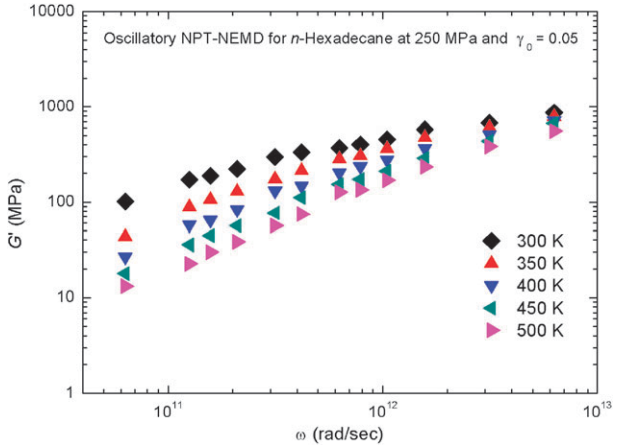

Fig. 11 Dependence of the frequency ω on the storage modulus G' at various temperatures for *n*-hexadecane under constant conditions (P = 250 MPa; γ_0 = 0.05).

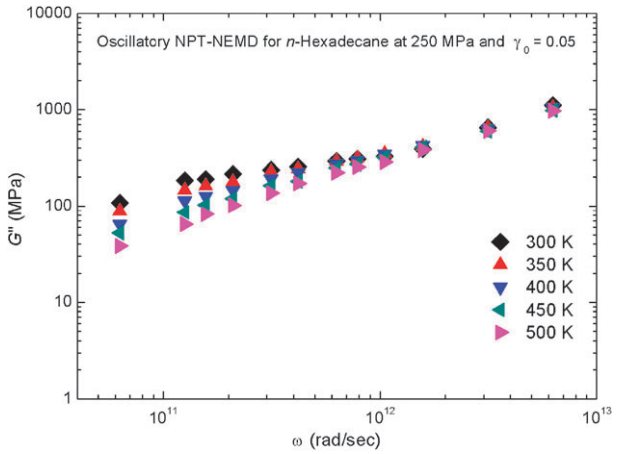

Fig. 12 Dependence of the frequency ω on the loss modulus G'' at various temperatures for *n*-hexadecane under constant conditions (P = 250 MPa; γ_0 = 0.05).

respectively. Additionally, the NEMD study of Guo *et al.*[79] also indicated that the viscosity at extreme shear rates remained virtually unchanged with respect to temperature.

Using the power-law model, $G' \propto \omega^{\alpha}$ and $G'' \propto \omega^{\beta}$, we fit both the $G'(\omega)$ and $G''(\omega)$ curves at $\omega \leq 6.28 \times 10^{11}$ rad s^{-1} to obtain the variations in the exponents α and β with respect to temperature. The values of α and β signify the rates of change of G' and G'' with respect to ω, respectively. Fig. 13 presents plots of α and β against T. Unexpectedly, we observe an intersection point near 375 K.

Referring to Fig. 9, the $\delta - T$ plot also features an intersection at *ca.* 375 K. Thereby, the variations of α and β were similar to that of δ. In other words, we tentatively suggest that α and β should be related to δ. As a result, the relationship between the exponent and the temperature could be also used to determine the so-called rheological states of the fluid: beyond the intersection the fluid is close to a pure viscous state; before it the fluid is viscoelastic.

D Thermorheological simplicity

Variations of the relaxation modulus with respect to time at different temperatures can obey the time–temperature

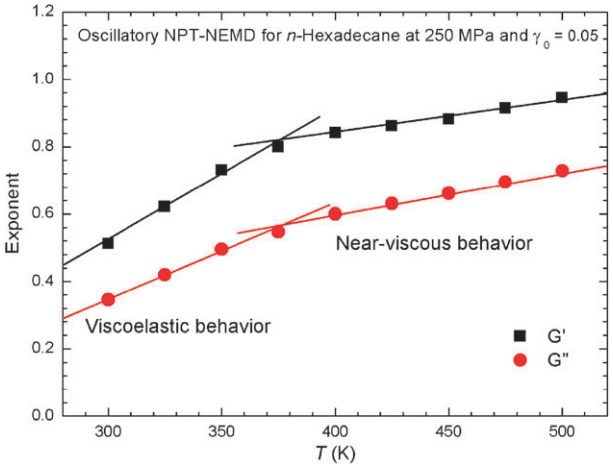

Fig. 13 Exponents of the power-law model ($G' \propto \omega^{\alpha}$ and $G'' \propto \omega^{\beta}$) plotted against the temperature T for *n*-hexadecane under constant conditions (P = 250 MPa; γ_0 = 0.05) over the frequency range $6.28 \times 10^{11} < \omega < 6.28 \times 10^{12}$ rad s^{-1}. Note that the two lines are linear fits of the data with an intersection appeared near 375 K.

superposition principle[1,9–11] to obtain one master curve at the reference temperature. Such fluids and materials are considered to exhibit thermorheological simplicity.[3,12–14] Therefore, the second—and significant—goal in the present study was to prove that the fluid possessed the characteristics of thermorheological simplicity.[1,9–11] Also, the Arrhenius flow activation energy was estimated.

1. Relaxation modulus master curve. For the time–temperature superposition principle,[1,9–11] the two shift factors are horizontal and vertical, a_T and b_T, respectively. The descriptor a_T is the shifting time or frequency variable; it is related to the relaxation time τ_R of molecules:

$$a_T = \frac{\tau_R(T)}{\tau_R(T_0)}, \tag{15}$$

where T_0 is the reference temperature. The descriptor b_T is the shifting modulus or compliance variable. It is related to the temperature and density:

$$b_T = \frac{\rho_0 T_0}{\rho T}, \tag{16}$$

where ρ_0 is the reference density.

Therefore, at T_0, the relaxation modulus $G(T_0)$ and time $t(T_0)$ variables can be given as,[1,11]

$$G(T_0) = b_T G(T), \tag{17}$$

$$t(T_0) = t(T)/a_T, \tag{18}$$

whereas for polymeric fluids, the value of b_T is assumed to be *unity* because variations in density with respect to temperature are not obvious.[11]

Note, however, that the length of the *n*-hexadecane molecule is shorter relative to that of a polymer. Hence, we must consider the effects of temperature and density on the value of b_T for *n*-hexadecane. Fig. 14 presents the $\rho(\omega)$ curves at various temperatures (300–500 K). The density decreased upon increasing the temperature, but it remained almost

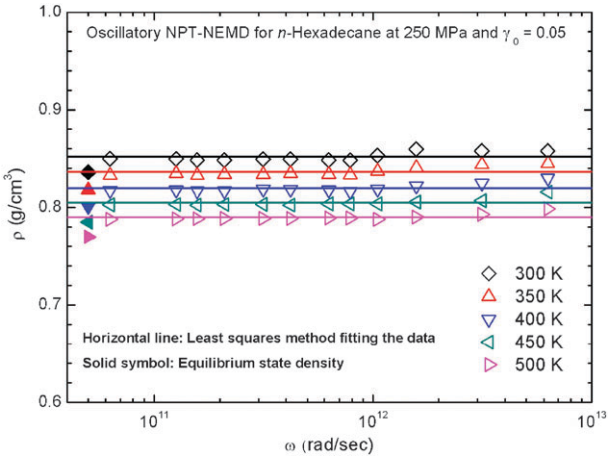

Fig. 14 Dependence of the frequency ω on the density ρ at various temperatures for *n*-hexadecane under constant conditions (P = 250 MPa; γ_0 = 0.05). The solid lines are curves fitted to the ρ–ω data using the least-squares method. Filled symbols indicate the equilibrium state points.

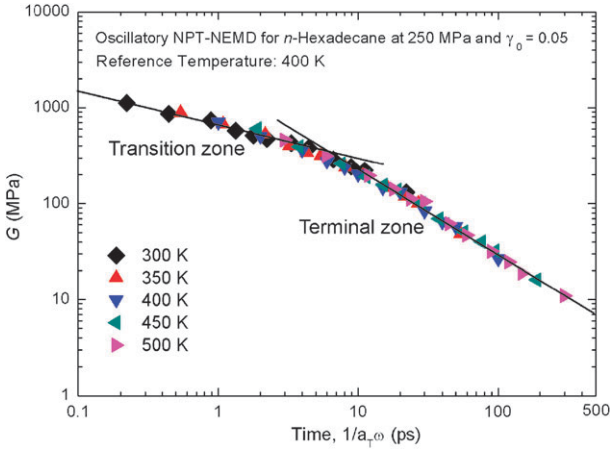

Fig. 15 Master curve of the relaxation modulus $G(t)$ as a function of the shifted time ($1/a_T\omega$) at a reference temperature of 400 K for *n*-hexadecane under constant conditions (P = 250 MPa; γ_0 = 0.05).

unchanged upon increasing the frequency—*i.e.*, we have evidence for the frequency independence of the density.

In steady state shear flow systems at low shear rates ($\dot{\gamma} < 1 \times 10^{11}$ s^{-1}),[27,49,50] the densities of *n*-hexadecane fluids in non-equilibrium states approximate those in equilibrium states. Conversely, at extreme shear rates ($\dot{\gamma} > 1 \times 10^{11}$ s^{-1}), the density decreases upon increasing the shear rate. This specific behavior is called *shear dilatancy*. We have explained the reason for its occurrence in a previous publication.[50] Therefore, the difference between the steady state and oscillatory shear flows is large, in terms of the variation in density, at non-equilibrium states.

Returning to Fig. 14, the solid lines and symbols indicate the convergent and equilibrium densities, respectively. The following convergent densities were obtained through least-squares fitting of the $\rho(\omega)$ curves: 0.852 g cm^{-3} (300 K), 0.836 g cm^{-3} (350 K), 0.820 g cm^{-3} (400 K), 0.805 g cm^{-3} (450 K), and 0.790 g cm^{-3} (500 K); the following equilibrium densities were determined as per our previous study:[27] 0.836 g cm^{-3} (300 K), 0.818 g cm^{-3} (350 K), 0.801 g cm^{-3} (400 K), 0.785 g cm^{-3} (450 K), and 0.770 g cm^{-3} (500 K).

Accordingly, we found that the convergent densities in non-equilibrium states under oscillatory shear were slightly larger than the equilibrium states densities. When the frequency approaches zero, the convergent densities should be close to those of the equilibrium states. Previously, we also obtained such a result in the steady state shear flow system.[27] In particular, Rah and Eu[80] discussed the effect of shear flow on a non-equilibrium liquid–vapor interface, while their results revealed that the liquid phase side density is also slightly increased, relative to the equilibrium density.

All linear viscoelastic properties can be related to the relaxation modulus.[1,2,5,9] According to Ferry's treatises[1] on polymer viscoelasticity, the relaxation modulus with respect to time, $G(t)$, simply approaches the storage modulus spectrum, namely,

$$G(t) \approx G'(1/\omega), \qquad (19)$$

where the time variable t is the inverse of the frequency ω (*i.e.*, $t = 1/\omega$).

Through the time–temperature superposition principle[1,9–11] and the approximation expression above, the storage modulus spectrum, recorded at different temperatures in Fig. 11, can be reduced to the master curve of the relaxation modulus, with respect to time at the reference temperature (T_0 = 400 K) in Fig. 15. Notably, Table 2 lists the shift factors of a_T with respect to temperature.

As a result, Fig. 15 presents a turning point at *ca.* 6.0 ps, and both a transition zone and a terminal zone. Before the turning point, the fluid existing in the transition zone was viscoelastic; beyond the turning point, the fluid in the terminal zone was viscous. Experimentally, referring to Ferry's polymer viscoelastic treatises,[1] the master curve for short polymer chains (amorphous polymers of low molecular weight) also exhibited both transition and terminal zones. Thereby, our master curve for *n*-hexadecane can be deemed qualitatively acceptable.

The complete relaxation modulus curve of polymeric materials features four zones: glassy plateau, transition, rubber plateau, and terminal zones.[5,11] Our $G(t)$ master curve revealed terminal and transition zones, but no glassy plateau and/or rubber plateau zones. At 400 K, our *n*-hexadecane fluid was in a liquid-like state; therefore, no glassy plateau occurred. A rubber plateau would be expected in the $G(t)$ curve if entanglement of the molecular chains occurred. Foteinopoulou *et al.*[81] demonstrated that once the chain length of polyethylene reaches *ca.* 200 UA, it begins to generate a degree of entanglement. Because *n*-hexadecane molecules would not exhibit such

Table 2 Shift factor a_T for various temperatures T in the master curve of the plot of the relaxation stress modulus $G(t)$ for *n*-hexadecane at a reference temperature of 400 K

T/K	a_T
300	4.500
350	1.850
400	1.000
450	0.525
500	0.335

obvious entanglement, it is clearly understandable that the $G(t)$ curve for *n*-hexadecane fluids did not feature a rubber plateau zone.

In particular, some researchers of polymer physics adopted coarse-grain molecular simulation technologies to perform the four-zone $G(t)$ master curve for polymeric fluids. Through the particular slip-link model and the efficient Green–Kubo technique adopted in equilibrium molecular dynamics (EMD) simulations, Likhtman *et al.*[82] presented the three-zone master curve for the entangled polymers, involving transition, rubber plateau, and terminal zones. Furthermore, Lin[83,84] and Das[84] employed Monte Carlo (MC) simulations for entanglement-free Fraenkel chains to also reveal the complete four-zone master curve, which agreed with rheological experimental data.[1,2,5,9]

2. Arrhenius flow activation energy. In a previous study regarding steady state shear flows of NEMD simulations,[27] we determined the Arrhenius flow activation energy, E_a = 10.99 kJ mol^{-1}, for *n*-hexadecane at 250 MPa, obtained *via* a plot of the zero-shear rate viscosity *versus* temperature. In the EMD results reported by Lee and Chang,[85] who discussed the viscosity and diffusion of various *n*-alkane molecules, the values of E_a for n-dodecane ($C_{12}H_{26}$) and *n*-icosane ($C_{20}H_{42}$) molecules were predicted to be 9.74 and 13.75 kJ mol^{-1}, respectively. Thus, through extrapolation, we would expect that the value for *n*-hexadecane ($C_{16}H_{26}$) molecules would be *ca.* 11.73 kJ mol^{-1}. In earlier experimental measurements, Dorrance *et al.*[86] used the fluorescence depolarization equipment to obtain the value of E_a by the values of the polarization plotted against temperature, namely, E_a = 16.00 kJ mol^{-1} for liquid *n*-hexadecane.

In the present study, we used the oscillatory shear data of a_T *versus* T (Table 2) to estimate the flow activation energy. Such a method is often adopted in polymer rheological experiments.[87] In general, the temperature-dependent shift factor (a_T) is determined by the Arrhenius equation,[87,88] as follows:

$$a_T = a_R \exp\left(\frac{E_a}{RT}\right), \qquad (20)$$

where a_R is the reference shift factor, E_a is the flow activation energy, T is the absolute temperature, and R is the gas constant (8.314 J mol^{-1} K).

As indicated in Fig. 16, the flow activation energy can be found by plotting the relationship between log a_T and 1000/T; wherein the slope of this line was 0.844. By using the Arrhenius equation, the flow activation energy, E_a = slope × ln 10 × 1000R, can be estimated to obtain a value of 16.16 kJ mol^{-1}. Unlike the previous value (10.99 kJ mol^{-1}) obtained by the steady shear flow,[27] therefore, this present value (16.16 kJ mol^{-1}) obtained by the oscillatory shear flow is very close to the prior experimental data (16.00 kJ mol^{-1}),[86] although certain conditions may be somewhat different.

IV. Conclusion

The ultimate goal of this article, which underlies modern NEMD methodology, is to present three clear rheological

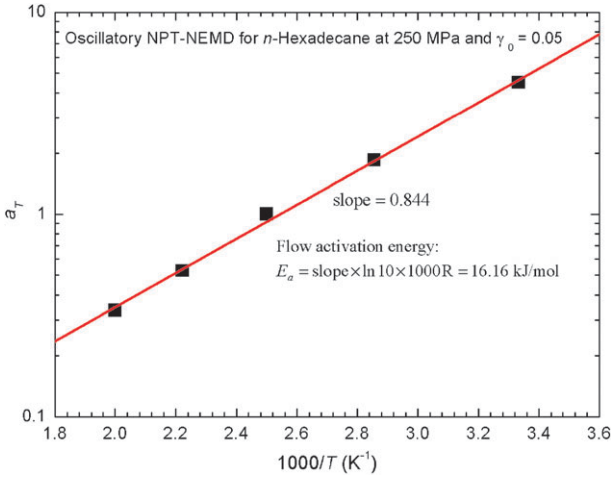

Fig. 16 Semi-logarithmic Arrhenius plot of the shift factor a_T as a function of the temperature T for *n*-hexadecane under isobaric conditions (P = 250 MPa). Note that the line is a fit to the data with the slope of 0.844.

pictures for the oscillatory sheared *n*-hexadecane fluid, namely, phase shift, linear viscoelasticity, and thermo-rheological simplicity. Overall, the fluid exhibits linear viscoelasticity in a suitable range of strain amplitudes, 0.01 ≤ γ_0 ≤ 0.1; whereas at high strain amplitudes, γ_0 > 0.1, the fluid exhibited a non-linear viscoelastic behavior of strain thinning. As the temperature rose, the range of linear viscoelasticity increased and the slope of strain thinning decreased.

The relaxation modulus curves, recorded at different temperatures (300–500 K), obeyed the time–temperature superposition principle to obtain one master curve at the reference temperature of 400 K, which featured both transition and terminal zones. In addition, the Arrhenius flow activation energy, 16.16 kJ mol^{-1}, was determined through the principle's shift factors. Those results are quite acceptable in comparison to related rheological experiments.

The viscoelastic spectrum, $G'(\omega)$ and $G''(\omega)$, increased upon increasing the frequency ω, but decreased upon increasing the temperature. Furthermore, we can distinguish phase states of the fluid at various temperatures. At the lowest temperature of 250 K, $G' > G''$ indicated that the fluid probably existed in a pure solid-like state. At 300 K, which is close to the melting temperature of *n*-hexadecane, $G' \approx G''$ signified a gel-like state. At 350 K, the liquid- and gel-like states coexisted over the whole range of frequencies. At such a temperature, the fluid's molecular chains at high frequencies possessed dynamics similar to Rouse chain dynamics. This is significant due to our finding the appropriate condition of the Rouse chain. When the fluid existed at high temperatures (>400 K), $G' < G''$ signifying a pure liquid-like state. Eventually, for non-equilibrium thermodynamic states of the fluid under oscillatory shear, upon increasing the frequency, the variation in the density reached an almost constant value; also, the density was slightly greater than the equilibrium density.

In the near future, we will prove whether the so-called Cox–Merz rule applied on a micro-scale is valid, which is a well-known empirical relation in the rheological/viscoelastic research field. This rule suggests that the magnitude of the

complex viscosity is equal to the steady shear viscosity at corresponding values of frequency and shear rate. A species of complex molecular structures (*e.g.*, H, star, branched, and dendrimer shapes), simple bio-molecules, and even soft matters all strongly affect dramatic variations of viscoelastic properties which makes possible a very interesting topic that will be tackled *via* coarse-grain MD simulations.

Acknowledgements

We are very grateful to the reviewers for their valuable suggestions and thoughtful criticism. We thank the National Science Council of the Republic of China for financial support (Grant number: NSC98-2221-E-007-008-MY2) and CoreTech System Co., Ltd (Moldex3D).

References

1 J. D. Ferry, *Viscoelastic Properties of Polymers*, Wiley-Interscience, New York, 3rd edn, 1980.
2 R. B. Bird, R. C. Armstrong and O. Hassager, *Fluid Mechanics*, Wiley-Interscience, New York, 2nd edn, 1987, vol. 1.
3 R. G. Larson, *Constitutive Equations for Polymer Melts and Solutions*, Butterworths, Boston, 1988.
4 C. W. Macosko, *Rheology: Principles, Measurements, and Applications*, VCH Publishers, New York, 1994.
5 J. M. Dealy and K. F. Wissbrun, *Melt Rheology and its Role in Plastics Processing*, Kluwer Academic Publishers, Dordrecht, 1999.
6 R. G. Larson, *The Structure and Rheology of Complex Fluids*, Oxford University Press, New York, 1999.
7 F. A. Morrison, *Understanding Rheology*, Oxford University Press, New York, 2001.
8 S. Tariq, A. J. Giacomin and S. Gunasekaran, *Biorheology*, 1998, **35**, 171.
9 D. Auhl, J. Ramírez, A. E. Likhtman, P. Chambon and C. Fernyhough, *J. Rheol.*, 2008, **52**, 801.
10 L. H. Sperling, *Introduction to Physical Polymer Science*, Wiley-Interscience, New York, 2nd edn, 1992.
11 M. T. Shaw and W. J. MacKnight, *Introduction to Polymer Viscoelasticity*, Wiley-Interscience, Hoboken, 3rd edn, 2005.
12 F. Schwarzl and A. J. Staverman, *J. Appl. Phys.*, 1952, **23**, 838.
13 Y.-H. Lin, *J. Phys.: Condens. Matter*, 2007, **19**, 466101.
14 E. T. J. Klompen and L. E. Govaert, *Mech. Time-Depend. Mater.*, 1999, **3**, 49.
15 M. P. Allen and D. J. Tildesley, *Computer Simulation of Liquid*, Clarendon Press, Oxford, 1989.
16 R. J. Sadus, *Molecular Simulation of Fluids*, Elsevier, New York, 1999.
17 D. J. Evans and G. P. Morriss, *Statistical Mechanics of Non-equilibrium Liquids*, Cambridge University Press, Cambridge, 2008.
18 D. M. Heyes, *J. Chem. Soc., Faraday Trans. 2*, 1986, **82**, 1365.
19 D. J. Evans and G. P. Morriss, *Phys. Rev. Lett.*, 1986, **56**, 2172.
20 A. Berker, S. Chynoweth, U. C. Klomp and Y. Michopoulos, *J. Chem. Soc., Faraday Trans.*, 1992, **88**, 1719.
21 S. Chynoweth and Y. Michopoulos, *Mol. Phys.*, 1994, **81**, 133.
22 R. Khare, J. de Pablo and A. Yethiraj, *J. Chem. Phys.*, 1997, **107**, 6956.
23 L. I. Kioupis and E. J. Maginn, *J. Phys. Chem. B*, 2000, **104**, 7774.
24 S. Bair, C. McCabe and P. T. Cummings, *Phys. Rev. Lett.*, 2002, **88**, 058302.
25 C. McCabe, C. W. Manke and P. T. Cummings, *J. Chem. Phys.*, 2002, **116**, 3339.
26 C. Baig, B. Jiang, B. J. Edwards, D. J. Keffer and H. D. Cochran, *J. Rheol.*, 2006, **50**, 625.
27 H.-C. Tseng, J.-S. Wu and R.-Y. Chang, *J. Chem. Phys.*, 2008, **129**, 014502.
28 S. Balasubramanian, C. J. Mundy and M. L. Klein, *J. Chem. Phys.*, 1996, **105**, 11190.
29 D. R. Wheeler and R. L. Rowley, *Mol. Phys.*, 1998, **94**, 555.
30 D. J. Evans, *Phys. Rev. A: At., Mol., Opt. Phys.*, 1981, **23**, 1988.
31 C. Baig, B. J. Edwards, D. J. Keffer, H. D. Cochran and V. A. Harmandaris, *J. Chem. Phys.*, 2006, **124**, 084902.
32 M. L. Matin, P. J. Daivis and B. D. Todd, *J. Chem. Phys.*, 2000, **113**, 9122.
33 J. M. Kim, D. J. Keffer, M. Kröger and B. J. Edwards, *J. Non-Newtonian Fluid Mech.*, 2008, **152**, 168.
34 C. Baig, B. J. Edwards, D. J. Keffer and H. D. Cochran, *J. Chem. Phys.*, 2005, **122**, 114103.
35 J. G. H. Cifre, S. Hess and M. Kröger, *Macromol. Theory Simul.*, 2004, **13**, 748.
36 K. Yoshimoto, T. S. Jain, P. F. Nealey and J. J. de Pablo, *J. Chem. Phys.*, 2005, **122**, 144712.
37 Q. Guo and M. S. Jhon, *IEEE Trans. Magn.*, 2006, **42**, 2540.
38 M. Vladkov and J.-L. Barrat, *Macromol. Theory Simul.*, 2006, **15**, 252.
39 J. S. Hansen, P. J. Daivis and B. D. Todd, *J. Chem. Phys.*, 2007, **126**, 144706.
40 Y.-G. Tao, I. O. Götze and G. Gompper, *J. Chem. Phys.*, 2008, **128**, 144902.
41 R. Khare, J. J. de Pablo and A. Yethiraj, *J. Chem. Phys.*, 2001, **114**, 7593.
42 G. Raos, M. Moreno and S. Elli, *Macromolecules*, 2006, **39**, 6744.
43 I. Borzsák and P. T. Cummings, *Phys. Rev. E: Stat. Phys., Plasmas, Fluids, Relat. Interdiscip. Top.*, 1997, **56**, R6279.
44 Y.-L. Chen, M. D. Graham, J. J. de Pablo, K. Jo and D. C. Schwartz, *Macromolecules*, 2005, **38**, 6680.
45 J.-C. Wang and K. A. Fichthorn, *J. Chem. Phys.*, 1998, **109**, 10138.
46 B. Bhushan, J. N. Israelachvili and U. Landman, *Nature*, 1995, **374**, 607.
47 R. C. Coy, *Tribol. Int.*, 1998, **31**, 563.
48 S. T. Cui, S. A. Gupta, P. T. Cummings and H. D. Cochran, *J. Chem. Phys.*, 1996, **105**, 1214.
49 H.-C. Tseng, J.-S. Wu and R.-Y. Chang, *J. Chem. Phys.*, 2009, **130**, 084904.
50 H.-C. Tseng, J.-S. Wu and R.-Y. Chang, *J. Chem. Phys.*, 2009, **130**, 164515.
51 K. Hyun, S. H. Kim, K. H. Ahn and S. J. Lee, *J. Non-Newtonian Fluid Mech.*, 2002, **107**, 51.
52 S. Toxvaerd, *J. Chem. Phys.*, 1988, **89**, 3808.
53 S. Fujiwara and T. Sato, *J. Chem. Phys.*, 1997, **107**, 613.
54 S. Chynoweth, R. C. Coy and Y. Michopoulos, *Proc. Inst. Mech. Eng., Part J: J. Eng. Tribol.*, 1995, **209**, 243.
55 A. Jabbarzadeh, J. D. Atkinson and R. I. Tanner, *Tribol. Int.*, 2002, **35**, 35.
56 A. Jabbarzadeh, J. D. Atkinson and R. I. Tanner, *J. Non-Newtonian Fluid Mech.*, 1998, **77**, 53.
57 A. Jabbarzadeh, J. D. Atkinson and R. I. Tanner, *J. Chem. Phys.*, 1999, **110**, 2612.
58 H.-C. Tseng, J.-S. Wu and R.-Y. Chang, *Mol. Simul.*, 2009, **35**, 691.
59 D. N. J. White and M. J. Bovill, *J. Chem. Soc., Perkin Trans. 2*, **1977**, 1610.
60 J. P. Ryckaert and A. Bellemans, *Chem. Phys. Lett.*, 1975, **30**, 123.
61 D. J. Evans and G. P. Morriss, *Comput. Phys. Rep.*, 1984, **1**, 297.
62 W. G. Hoover, D. J. Evans, R. B. Hickman, A. J. C. Ladd, W. T. Ashurst and B. Moran, *Phys. Rev. A: At., Mol., Opt. Phys.*, 1980, **22**, 1690.
63 A. W. Lees and S. F. Edwards, *J. Phys. C: Solid State Phys.*, 1972, **5**, 1921.
64 R. Edberg, G. P. Morriss and D. J. Evans, *J. Chem. Phys.*, 1987, **86**, 4555.
65 K. P. Travis, P. J. Daivis and D. J. Evans, *J. Chem. Phys.*, 1995, **103**, 1109.
66 D. Macgowan and D. M. Heyes, *Mol. Simul.*, 1988, **1**, 277.
67 J. H. Ferziger and M. Peric, *Computational Methods for Fluid Dynamics*, Springer Science, Berlin, 3rd edn, 2002.
68 J. H. Irving and J. G. Kirkwood, *J. Chem. Phys.*, 1950, **18**, 817.
69 W. H. Press, S. A. Teukolsky, W. T. Vetterling and B. P. Flannery, *Numerical Recipes in C*, Cambridge University Press, New York, 3rd edn, 2007.
70 K. Hyun, J. G. Nam, M. Wilhelm, K. H. Ahn and S. J. Lee, *Korea-Aust. Rheol. J.*, 2003, **15**, 97.
71 J. G. Oakley, A. J. Giacomin and J. A. Yosick, *Mikrochim. Acta*, 1998, **130**, 1.

72 R. S. Jeyaseelan and A. J. Giacomin, *J. Non-Newtonian Fluid Mech.*, 2008, **148**, 24.
73 D. Chandler, *Introduction to Modern Statistical Mechanics*, Oxford University Press, New York, 1987.
74 C.-Y. M. Tung and P. J. Dynes, *J. Appl. Polym. Sci.*, 1982, **27**, 569.
75 Y. Tsuchiya, H. Hasegawa and T. Iwatsubo, *J. Chem. Phys.*, 2001, **114**, 2484.
76 J. M. Haile, *Molecular Dynamics Simulation*, Wiley-Interscience, New York, 2nd edn, 1997.
77 D. A. McQuarrie, *Statistical Mechanics*, University Science Books, Sausalito, 2000.
78 I.-K. Yang, P.-J. Wang and P.-H. Tsai, *J. Appl. Polym. Sci.*, 2007, **103**, 2107.
79 Q. Guo, P. S. Chung, H. Chen and M. S. Jhon, *J. Appl. Phys.*, 2006, **99**, 08N105.
80 K. Rah and B. C. Eu, *Phys. A*, 2001, **292**, 102.
81 K. Foteinopoulou, N. C. Karayiannis and V. G. Mavrantzas, *Macromolecules*, 2006, **39**, 4207.
82 A. E. Likhtman, S. K. Sukumaran and J. Ramírez, *Macromolecules*, 2007, **40**, 6748.
83 Y.-H. Lin, *Polymer Viscoelasticity*, World Scientific, London, 2003.
84 Y.-H. Lin and A. K. Das, *J. Chem. Phys.*, 2007, **126**, 074902.
85 S. H. Lee and T. Chang, *Bull. Korean Chem. Soc.*, 2003, **24**, 1590.
86 R. C. Dorrance, T. F. Hunter and J. Philp, *J. Chem. Soc., Faraday Trans. 2*, 1977, **73**, 89.
87 C. A. Solunov and C. S. Ponevsky, *J. Polym. Sci., Polym. Phys. Ed.*, 1977, **15**, 969.
88 P. Wood-Adams and S. Costeux, *Macromolecules*, 2001, **34**, 6281.